Journal of the Mechanics and Physics of Solids 98 (2017) 1–11

Contents lists available at ScienceDirect

Journal of the Mechanics and Physics of Solids

journal homepage: www.elsevier.com/locate/jmps

A Dynamic Discrete Dislocation Plasticity study of elastodynamic shielding of stationary cracks

B. Gurrutxaga-Lerma [a,*], D.S. Balint [a], D. Dini [a], A.P. Sutton [b]

[a] Department of Mechanical Engineering, Imperial College London, Exhibition Road, SW7 2AZ London, United Kingdom
[b] Department of Physics, Imperial College London, Exhibition Road, SW7 2AZ London, United Kingdom

ARTICLE INFO

Article history:
Received 22 January 2016
Received in revised form
16 May 2016
Accepted 25 August 2016
Available online 13 September 2016

ABSTRACT

Employing Dynamic Discrete Dislocation Plasticity (D3P), an elastodynamic analysis of the shielding of a stationary crack tip by dislocations is studied. Dislocations are generated via Frank–Read sources, and make a negligible contribution to the shielding of the crack tip, whereas dislocations generated at the crack tip via homogeneous nucleation dominate the shielding. Their effect is found to be highly localised around the crack, leading to a magnification of the shielding when compared to time-independent, elastostatic predictions. The resulting attenuation of $K_I(t)$ is computed, and is found to be directly proportional to the applied load and to $\sqrt{t}$.

1. Introduction

Plastic flow at a crack tip is a possible relaxation mechanism because of the large elastic stresses experienced by the material in its vicinity, which may be reduced by the generation and motion of dislocations (Freund, 1989; Thomson, 1986). The power dissipated in the active plastic region depends on the microscopic processes governing the plastic flow, as well as the local nature of the crystal structure; both of these are known to be affected by the strain rate and the applied stress levels, amongst other parameters (Meyers, 1994).

The active plastic region is determined by the generation and motion of dislocations, the fields of which may shield the crack tip, i.e., relax the magnitude of the elastic field in the environs of the crack tip, whereby an increased shielding leads to increased apparent fracture toughness. Plastic shielding of crack tips under quasi-static loading has been treated experimentally (Samuels and Roberts, 1989; George and Michot, 1993), in continuum models using constitutive laws of plasticity (Thompson, 1987; Jokl et al., 1980, 1989; Rice, 1987; Tvergaard and Hutchinson, 1992; Rice and Beltz, 1994), in theoretical studies of the interaction between the crack tip and dislocations (Hirsch et al., 1989; Hirsch and Roberts, 1996; Loyola de Oliveira and Michot, 1998), in elastostatic discrete dislocation dynamics studies of the collective effect of individual dislocations over the crack tip (Cleveringa et al., 2000; O'Day and Curtin, 2005; Balint et al., 2005), and in atomistic simulations (Bulatov et al., 1998; Holland and Marder, 1998; Kermode et al., 2008, 2013).

The study of plastic shielding under dynamic loading conditions has also received a great deal of attention, particularly through experimental studies of the evolution of the fracture toughness with crack speed (Kalthoff and Shockey, 1977; Homma et al., 1983; Klepaczko, 1990) and theoretical and numerical analyses of plastic shielding via constitutive modelling of rate-dependent plasticity (Freund and Hutchinson, 1985; Freund, 1989). Nevertheless, the way in which the

* Correspondence to: Department of Engineering, University of Cambridge, Trumpington St, Cambridge CB2 1PZ, United Kingdom.
E-mail address: bg374@cam.ac.uk (B. Gurrutxaga-Lerma).

http://dx.doi.org/10.1016/j.jmps.2016.08.014
0022-5096/

elastodynamic fields of dislocations may shield the crack tip and, therefore, the specific way in which a dynamic crack tip is plastically relaxed has not been studied in detail.

Dynamic fracture is characterised by external loads intense enough to propagate the crack tip at a significant fraction of the Rayleigh wave speed (Freund, 1989). For cracks to grow by microns at speeds of the order of 10^3 m/s, the timescales involved in the plastic relaxation of a crack tip must be of the order of hundreds of picoseconds. During these brief periods of time, shielding dislocations around the crack tip will be subjected to large stresses, potentially leading to fast moving dislocations. Under these conditions, the propagation speeds of the elastic fields of dislocations will be of the same order of magnitude as those of the crack tip, which suggests that a fully time-dependent, elastodynamic analysis of crack tip shielding is required in order to account for the retardation affecting dislocation interactions with one another and with the crack.

Aside from retardation effects, previous elastodynamic studies of discrete dislocation dynamics (see Gurrutxaga-Lerma et al., 2015a,b) have shown that dislocations moving at speeds approaching the shear wave speed tend to magnify plastic relaxation effects locally due to inertial effects; this raises the question of whether the elastodynamic shielding of crack tips will similarly be subjected to magnifications. This article examines the dislocation shielding of stationary crack tips under dynamic conditions by employing *Dynamic Discrete Dislocation Plasticity* (D3P). This method enables a fully elastodynamic treatment of both the crack tip singularity and the interactions between the latter and individual dislocations. The aim of this article is to clarify the processes through which plastic shielding of a stationary crack tip occurs, and to determine whether it is enough to lead to increased fracture toughness under dynamic conditions. The focus here on the stationary crack is a first step towards building a clear understanding of the way the shielding exerted by elastodynamic dislocations differs from that of classical quasi-static dislocations.

2. Dynamic Discrete Dislocation Plasticity model of a stationary crack

D3P was developed by Gurrutxaga-Lerma et al. (2013) as the elastodynamic extension of Discrete Dislocation Plasticity (DDP) (Van der Giessen and Needleman, 1995). In D3P the dislocation's mutual interactions and the interactions between the dislocations and the boundary conditions are accounted for via their elastodynamic fields. This entails solving the Navier–Lamé equation for both the fields of dislocations and those due to the boundary conditions (Gurrutxaga-Lerma et al., 2013). Following Van der Giessen and Needleman (1995), Gurrutxaga-Lerma et al. (2013) proposed employing the linear superposition principle, where the analytic elastodynamic fields of non-uniformly moving, injected straight edge dislocations in an infinite plane can be employed in conjunction with an elastodynamic finite element numerical solver for the boundary conditions. Dislocation generation and motion follow the rules defined in Gurrutxaga-Lerma et al. (2014).

The present study focuses solely on FCC aluminium, with elastic constants $\mu=28.3$ GPa and $E=63.2$ GPa, density $\rho=2700$ kg/m^3, and $B=2.85$ Å the magnitude of the Burgers vector. The dislocations glide in slip planes oriented at 54.7°, 125.2° and 0° (see Rice, 1987) with respect to the crack faces. The dislocations move with a mobility law extracted from molecular dynamics simulations of edge dislocations in aluminium (Olmsted et al., 2005), and given by (see Gurrutxaga-Lerma et al., 2015b),

$$\frac{d_0}{1-\frac{v_i^2}{c_R^2}}\cdot v_i = f_{PK}^i \tag{1}$$

where v_i is the ith dislocation's glide speed and f_{PK}^i the magnitude of the glissile component of the Peach–Koehler acting on it. In order to prevent elastodynamic resonances with the free surfaces (Gurrutxaga-Lerma et al., 2015c), the effective limiting speed in Eq. (1) is made to be c_R, the Rayleigh wave speed (here, around $0.98c_t$). For glide speeds v significantly lower than c_R, Eq. (1) behaves almost linearly with respect to v; thus, d_0 can be interpreted as a linear drag coefficient (cf. Hirth and Lothe, 1982); the data fit from Olmsted et al. (2005) renders $d_0 = 2\cdot10^{-5}$ Pa s, in good agreement with the expected linear drag coefficient in aluminium (Balint et al., 2005).

The glissile component of Peach–Koehler force is computed as (Van der Giessen and Needleman, 1995)

$$f_{PK}^i = n_k^i\left(\sum_{j\neq i}\tilde{\sigma}_{kl}^j + \hat{\sigma}_{kl}\right)B_l^i \tag{2}$$

where $\tilde{\sigma}_{kl}^j$ is the elastodynamic stress field component due to the j-th dislocation in an infinite plane (the expressions of which can be found in Gurrutxaga-Lerma et al., 2013), and $\hat{\sigma}_{kl}$ is the elastodynamic stress field correction due to the boundary conditions (Van der Giessen and Needleman, 1995); n_k is the i-th dislocation's normal to the slip plane, and B_l^i is the i-th dislocation's Burgers vector l-th component. Here B is used instead of the usual b to denote the magnitude of the Burgers vector to avoid confusion with b, the transverse slowness of sound.

The geometry and boundary conditions employed in this study are shown in Fig. 1. The 4×4 μm system consists of a crack of length 2 μm, with the crack tip occupying the central position of the sample. A constant tensile load per unit area of magnitude P is applied on the bottom surface, whilst the top surface is subjected to reflective boundary conditions; all other

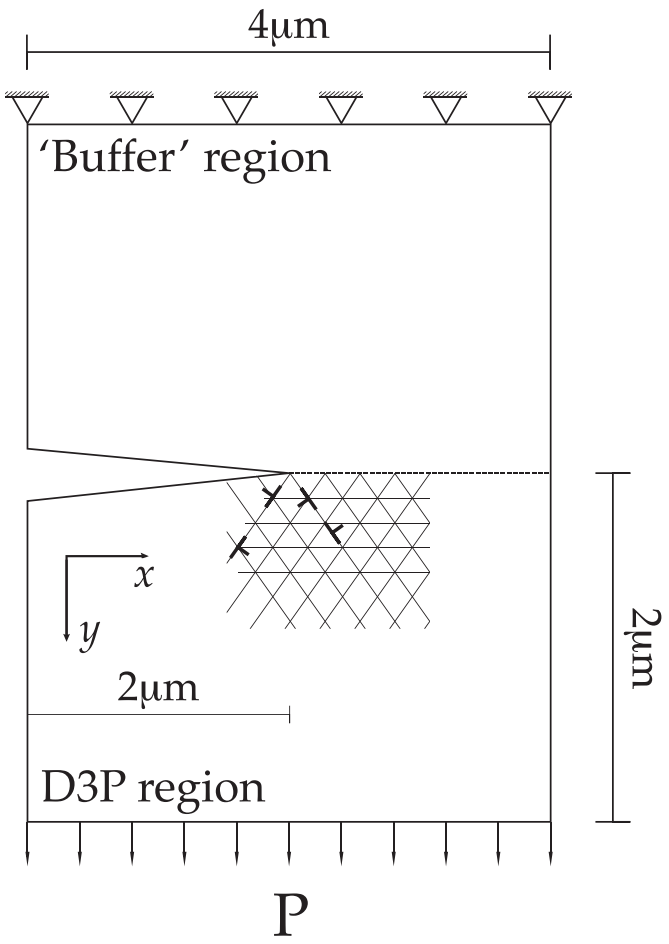

Fig. 1. Geometry of the simulated system. The lower D3P region concentrates the dislocation activity; the 'buffer' region is dislocation free, and is employed to avoid spurious reflections of the incoming elastic waves along the crack path.

surfaces are free surfaces. The system is pre-loaded and dislocation-free; this is to avoid the complexities arising from a fully transient elastodynamic loading, where a wavefront would need to propagate through the system in an asymmetrical fashion (Freund, 1989). Thus, at the beginning of the simulation the whole system is subjected to the stationary elastic field of the crack caused by the external loading P. As the simulation begins, and as a result of the loading and the subsequent crack tip stress field, dislocation generation and motion is triggered; these dislocations are treated elastodynamically employing D3P, whilst thereafter the associated boundary value problem is solved employing a finite element method elastodynamic solver.

The D3P simulation is carried out over the lower half-plane alone (see Fig. 1) to reduce its computational cost. This is a standard practice in DDP simulations of cracks (see Cleveringa et al., 2000; O'Day and Curtin, 2005; Balint et al., 2005). The D3P simulation consists of a lower D3P region, where dislocation activity takes place, and an upper 'buffer' region in which dislocation activity is not allowed, but through which elastic waves can travel. Unlike in elastostatic DDP simulations (vid. Cleveringa et al., 2000; O'Day and Curtin, 2005; Balint et al., 2005), enabling a symmetry boundary condition along the crack path would lead to unrealistic wave reflections from the crack path; the buffer region enables wave transmission through the crack path, and prevents unrealistic interactions with the boundaries. Dislocations leaving the D3P region for the buffer region are pinned as virtual dislocations (see Gurrutxaga-Lerma et al., 2014) in the position they reach at the end of the time step.

2.1. Generation of dislocations

2.1.1. Frank–Read sources

The usual mechanism for the generation of dislocations in planar dislocation dynamics is the Frank–Read source (Van der Giessen and Needleman, 1995). In the D3P simulations under consideration here, Frank–Read sources are randomly distributed with a density 100 sources per μm^2 throughout the D3P region (Van der Giessen and Needleman, 1995). This is a common value found in DDP simulations (Balint et al., 2005, 2006; Benzerga, 2009; Davoudi et al., 2014; Nicola et al., 2001,

2003); no physical argument to impose a much larger source density can be invoked without assuming the material has been subjected to prior loading (e.g., being cold-worked). The Frank–Read sources represent a pre-existing density of pinned dislocation segments, which enable yielding once the resolved shear stress over a source exceeds the source strength, τ_{nuc}, which is the stress required for a Frank–Read source segment to reach its critical position (see Benzerga, 2008, 2009; Shishvan and Van der Giessen, 2010; Gurrutxaga-Lerma et al., 2015d). The source strength is related to the pinned segment's length l_{FR} (Shishvan and Van der Giessen, 2010); in the simulations considered here, it is made to be normally distributed with mean $\bar{\tau}_{FR} = 100$ MPa and standard deviation 1 MPa.

A dipole is injected into the system if the source strength is met or exceeded for a sufficiently long time t_{nuc}. The introduction of a *nucleation time* for Frank–Read sources is a requirement of the dynamics of the bowing segment (Benzerga, 2008; Gurrutxaga-Lerma et al., 2015d): from the original unbowed position, the Frank–Read source segment requires time to reach its critical position. As was done in Gurrutxaga-Lerma et al. (2015a,b), the mechanics of the bowing segment and, consequently, the activation time of the Frank–Read sources is calculated numerically from a model adapted from Gurrutxaga-Lerma et al. (2015d).

The model employed here tracks the position of the central bowing segment, $h(t)$, relative to its unbowed position. This segment must satisfy a force balance between the applied stress, the lattice resistance to the motion of the dislocation (i.e., the drag force), and as the segment acquires curvature, the dislocation's line tension. The activation time is defined as the time t_{nuc} for which the central segment reaches the critical position, which is approximated as $h_c = l_{\mathrm{FR}}/2$ (vid. Benzerga et al., 2004). This requires solving for $h(t)$ in the following equation:

$$\tau B = \frac{d_0}{1 - \dfrac{(dh(t)/dt)^2}{c_t^2}} + \frac{\mu B^2}{\dfrac{h(t)}{2} + \dfrac{l_{\mathrm{src}}^2}{8h(t)}} \tag{3}$$

where τ is the applied stress. The first term on the right hand side is the drag force the segment experiences as it bows out, corresponding to the mobility law defined in Eq. (1); the same parameters as those defined in Section 2 above are used here. The second term on the right hand side of Eq. (3) represents the line tension assuming that the bowing segment has circumferential curvature. This is an approximation that both Benzerga (2008) and Gurrutxaga-Lerma et al. (2015d) have shown to be of little consequence in computing the activation times, despite the fact that the actual shape the bowing segment tends to adopt is oval (Gurrutxaga-Lerma et al., 2015d). Consequently, the nucleation criteria that the nucleation time t_{nuc} corresponds to the time it takes for the central segment to reach the critical position $h(t_{\mathrm{nuc}}) = l_{FR}/2$ merely prescribe a critical shape for the Frank–Read source segment of a perfect semi-circumference; this is a reasonable approximation because the curvature of the central dislocation segment is approximately circular throughout the bowing process.

In the simulations presented here, Eq. (3) is solved numerically for a given applied τ, computed as the aggregate contribution of all individual dislocations and boundary conditions; l_{src} is obtained from the source strength, as (Brown, 1964)

$$l_{\mathrm{src}} = \beta \frac{\mu B}{\tau_{\mathrm{FR}}} \tag{4}$$

where in turn

$$\beta = \frac{A}{2\pi}\left[\ln \frac{l_{\mathrm{src}}}{r_0} + C\right] \tag{5}$$

and $A=1$, $C=-3.4$ for aluminium (Gurrutxaga-Lerma et al., 2015d), and r_0 the dislocation's core cut-off radius ($10B$).

All other injection rules follow those defined in Gurrutxaga-Lerma et al. (2015d). In particular, Frank–Read source activation results in the injection of a dipole of edge dislocations, with an equilibrium spacing given by (Gurrutxaga-Lerma et al., 2015d):

$$L_{\mathrm{nuc}} = \frac{B\mu}{\pi\tau b^2} \frac{4s^2\sqrt{s^2-a^2}\sqrt{s^2-b^2} - b^4 + 4b^2s^2 - 4s^4}{s\sqrt{s^2-b^2}} \tag{6}$$

where $a = 1/c_l$ and $b = 1/c_t$ are the longitudinal and transverse slownesses of sound, respectively; and $s = 1/v$ is the glide slowness.

2.1.2. Homogeneous nucleation at the crack tip

In the D3P framework, and provided that the material is annealed, free of any precipitates, phase interfaces or grain boundaries, the simplest way of simulating the generation of dislocations at the crack tip is by accepting that dislocations can be homogeneously nucleated at the tip. The homogeneous nucleation of dislocations at the crack tip, or lack thereof, has been studied in the context of the ductile–brittle transition in metals (Rice and Thomson, 1974; Hirsch et al., 1989). The possibility of homogeneous nucleation occurring has been discarded for a number of materials but supported for others (Rice and Thomson, 1974; Xu and Argon, 2000). Whenever there are particles, grain boundaries, precipitates or other discontinuities along the crack path, homogeneous nucleation is thought to be less likely than heterogeneous nucleation, as the latter entails lower activation stresses (Xu et al., 1997; Zhu et al., 2004), and is therefore thought to be dominant.

Nevertheless, under stress conditions similar to those found at a crack tip (e.g. nano-indentations), homogeneous nucleation has been reported experimentally (Minor et al., 2006), and recent atomistic studies also support its existence at lower applied stresses than originally thought (Gutkin and Ovidko, 2008; Tschopp and McDowell, 2007, 2008; Aubry et al., 2011).

Since it is not the aim of this article to determine whether homogeneous nucleation is the governing mechanism behind the ductile–brittle transition but, rather, to examine the elastodynamic shielding effects over the crack tip, homogeneous nucleation is included here primarily as a physically motivated device for injecting dislocations into the system in the immediate vicinity of the crack tip.

In the D3P simulations reported here, the homogeneous nucleation of dislocations is implemented following the rules defined by Gurrutxaga-Lerma et al. (2015b). Upon overcoming a threshold stress of $\tau_{\text{nuc}} = \mu/(4\pi)$, a dipole is instantaneously injected (i.e., injected during the same time step the source is activated); this threshold stress corresponds with the theoretical lattice shear strength of the material, usually assumed to be somewhere between $\mu/(4\pi)$ and $\mu/18$. It must be noted that the dislocation's core cut-off distance is chosen to be $r_c = 10B$; the radial stress within the core matches that at the cut-off distance (Gurrutxaga-Lerma et al., 2013). This ensures that the stresses within the core always remain below the lattice shear strength; thus dislocations can only (albeit unlikely) generate other dislocations homogeneously through long-range interactions—this ensures that avalanches of homogeneously nucleated dislocations do not take place. The homogeneous injection distance (i.e., the separation between the two dislocations in the newly injected dipole) follows a rare event Poisson distribution with $\lambda = 5B$ (where λ is the expected value), which entails that some dipoles collapse back onto each other. Any point in the material subjected to these stresses is considered a possible nucleation site, albeit the nucleation sites are spaced $10B$ to prevent newly injected dipoles from overlapping. This exclusion zone only applies to lattice locations, and remains unaffected by the presence of a dislocation.

Additional generation mechanisms are not considered in this work. This means that the effects described in the following D3P dislocations will generally apply over short timescales and to annealed, pure materials. Although homogeneous nucleation at the crack tip may be unlikely if precipitates or impurities are present, a different nucleation process (e.g., heterogeneous nucleation) would probably not cause a radically different elastodynamic response with respect to crack shielding, provided that it operates on a similar time scale and there are enough alternative nucleation sites available. Furthermore, particularly at the highest loading rates, it seems unlikely that heterogeneous sources could be sufficiently numerous to effectively shield the crack enough to prevent homogeneous nucleation within the timescales involved.

3. Results and discussion

In the D3P simulations reported here, the system is subjected to three different loads, $P = 500$ MPa, $P = 1$ GPa, $P = 1.5$ GPa; this is to ensure that the loading remains relevant to dynamic fracture (cf. Freund, 1989). As expected, the stress field is locally magnified at the crack tip (Freund, 1989), leading to stress conditions that, albeit caused by loads much lower than those attained in high strain rate shock loading, are of similar magnitude and take place over similar timescales. Such loading affects both the activation time of Frank–Read sources, which is governed by Eq. (3), and the region where homogeneous nucleation is dominant due to the magnitude of the crack tip's elastic fields.

Irrespective of the magnitude of the loading, the simulations display a series of common characteristics summarised in

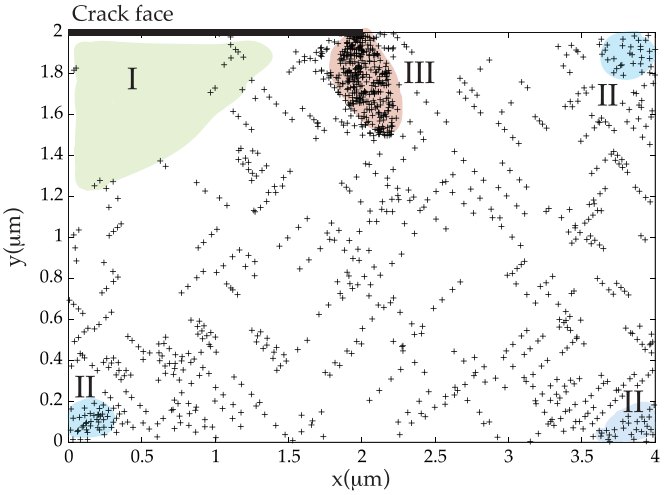

Fig. 2. Dislocation microstructure at 100 ps for a $P = 1$ GPa loading. Each cross '+' represents a dislocation. The crack tip is located at (2, 2) μm. Dislocations in region III are mostly homogeneously nucleated dislocations. Elsewhere, they are generated by Frank–Read sources that have been activated no more than twice within the first 100 ps of the simulation. (For interpretation of the references to colour in this figure caption, the reader is referred to the web version of this paper.)

Fig. 2. This figure shows the dislocation microstructure at 100 ps for a loading of $P=1$ GPa. Region I (highlighted in green) corresponds with the unloaded region under the lower crack face, and therefore barely any dislocation activity exists there. Region II (highlighted in blue) are the corners, which are subjected to geometrical effects and display a slightly larger dislocation density. The dislocation density is about two orders of magnitude higher around the crack tip in region III (highlighted in red, $\rho_{\text{dis}} \approx 10^{16}\ \text{m}^{-2}$), where homogeneous nucleation is the prevalent mechanism of dislocation generation in a proportion of ≈100: 1 homogeneous nucleation events vs Frank–Read source activations throughout the simulation. The size of region III increases in proportion to the loading, but the dislocation density remains of the same order of magnitude. This is because the larger the loading, the larger is the magnitude of the crack tip field, which propels existing shielding dislocations away from the crack tip.

Away from these regions, it is primarily Frank–Read sources that are activated. They prove insufficient to plastically relax the structure in the timescale of the simulation, and barely contribute to the shielding of the crack tip. This is because their collective 'background' shielding (cf. Hirsch and Roberts, 1996) is too weak compared to the relaxation requirements of the crack tip. Two factors may contribute to this weak effect.

On one hand, there is the rate at which the sources are activated. As described in Section 2.1, the activation of Frank–Read sources is characterised by a finite time, t_{nuc}, which depends on the source strength (or length), and on the external loading. Even in the most favourable scenario (that of the sources in the immediate vicinity of the crack tip) the activation time is too great: no smaller than about 40–160 ps. Under these conditions, the Frank–Read sources that are near enough to be able to influence the crack tip will do so at an extremely slow rate. Necessarily, their effect will be superseded by that of homogeneous nucleation at the crack tip.

On the other hand, the density of Frank–Read sources, representing a pre-existing dislocation density, is too small compared to that required to relax the crack tip. The value of $100\ \mu\text{m}^{-2}$ is representative of that found in other plasticity applications (see Van der Giessen and Needleman, 1995; Balint et al., 2005, 2006); as mentioned above, there is no *a priori* justification to assume it should be orders of magnitude larger than that. Nevertheless, the effect of an extremely large density of Frank–Read sources was tested by defining $\approx 10^6\ \text{m}^{-2}$ sources within a radial distance of $r = c_t \cdot 150$ ps from the crack tip (i.e., enough to influence the crack tip during the current simulations); it was found that the relaxation arising from $10^6\ \text{m}^{-2}$ sources is still unable to compete with the effect of homogeneous nucleations. This is because, again, the nucleation of new dislocations is limited by the rate at which Frank–Read sources can be activated: by the time the first burst of dislocations is generated (≈ 40 ps in the simulations), the crack tip has already been considerably relaxed by homogeneous nucleation. Thus, in this study most of the plastic relaxation at the crack tip is due to homogeneously nucleated dislocations.

As is characteristic of elastodynamic simulations of dislocation dynamics (vid. Gurrutxaga-Lerma et al., 2013, 2015a), the propagation time of the dislocation fields is of paramount importance in shielding the crack tip. Fig. 3(a) shows the relaxation of σ_{yy} along the crack path at 100 ps for $P=1$ GPa as obtained from the D3P simulation; here 'relaxation' refers to the contribution of the stress fields of the dislocations alone. Fig. 3(a) also shows the elastostatic plastic relaxation of σ_{yy} for the same configuration. The elastodynamic relaxation predicted by D3P is remarkably different from that of its elastostatic counterparts; the intensity is about 25% larger than in the elastostatic case. The dynamic enhancement of the relaxation remains throughout the simulation, and is one of the defining characteristics of the elastodynamic shielding observed in the present D3P simulations.

The elastodynamic magnification of the plastic relaxation at the crack tip is accompanied by additional effects that must be attributed to the wave-like nature of the elastodynamic fields of the dislocations. In Fig. 3(a) it can be clearly seen that the elastodynamic dislocations barely influence the field sufficiently ahead of the crack tip. This is because most of the crack tip relaxation is due to dislocations that are nucleated homogeneously at the tip, but their elastic fields, propagating at the speeds of sound (Gurrutxaga-Lerma et al., 2013), do not have time to reach the rear end of the crack path beyond approximately 2.5 μm, and therefore their effect remains concentrated at the tip. At the same time, as was discussed in Gurrutxaga-Lerma et al. (2014), the shape of the longitudinal component of the stress fields of dislocations (which is the fastest propagating component) is rather different to the stationary elastostatic fields; this prescribes a transient plastic relaxation of the crack path that, as shown in Fig. 3(a), will evolve rather differently from the elastostatic counterpart. Most remarkably, the elastostatic dislocations induce a positive (tensile) plastic stress along the crack path that is not present in the elastodynamic D3P description, which could be associated with the nucleation of voids and, hence, ductile fracture (Meyers, 1994); the elastodynamic response does not display such behaviour.

Frank–Read sources have little effect on the relaxation along the crack path: there is no statistically significant variation in the magnitude of the elastodynamic shielding at any of the loads studied here when Frank–Read sources are omitted from the simulations. This is shown in Fig. 3(b) for $P=1$ GPa and $t=50$ ps: in the vicinity of the crack tip, the relaxation remains statistically comparable. The same behaviour can be obtained for different loads and longer and shorter times. The plastic activity observed for $x > 3.5$ μm is due to Frank–Read sources activated as a result of the surface and geometrical effects (see region II in Fig. 2).

Fig. 4 shows contours of σ_{yy} due to the dislocations, only for the elastodynamic and elastostatic cases, at $t=100$ ps for $P=1$ GPa. Although qualitatively similar, the elastodynamic fields exhibit larger plastic localisation and stronger shielding both in the crack tip region surrounding and in the far-field background, where on average the elastodynamic σ_{yy} is more compressive than its elastostatic counterpart.

Nonetheless, as can be seen from comparing Figs. 4(a) and (b) the effect of the background dislocations (i.e., those relatively away from the crack tip) is similar in either case. This is attributed to the relative speeds of the dislocations. A

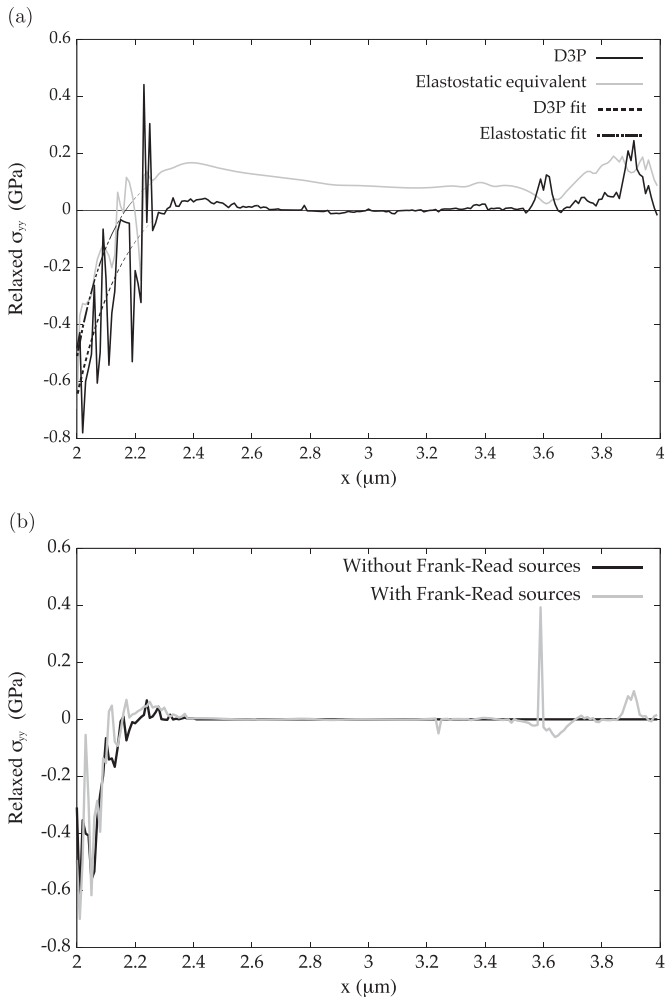

Fig. 3. Relaxation of σ_{yy} along the crack's path. (a) Relaxed σ_{yy} field along the crack path at 100 ps for $P=1$ GPa, showing the elastostatic relaxation that would have been exerted by the same configuration of dislocations. (b) Relaxed σ_{yy} field along the crack path at 50 ps for $P=1$ GPa, for simulations with and without Frank–Read sources.

detailed study of the frequency distribution of the speeds of the dislocations in the whole system shows that it approximately follows a Gaussian distribution; for instance, for $P=1$ GPa at $t=100$ ps the average speed of dislocations is $M_t \approx 0.5$ (where $M_t = v/c_t$ is the transverse Mach number), with a wide standard deviation of $M_t \approx 0.2$. Most high speed dislocations, understood as those with speeds in excess of $M_t=0.8$, are located in the vicinity of the crack tip. However, if one excludes the dislocations in regions II and III and focuses on those generated by Frank–Read sources, it is found that they move at relatively uniform speeds, with an average speed of $M_t \approx 0.2$ for 500 MPa, $M_t=0.3$ for 1 GPa and $M_t=0.35$ for 1.5 GPa, with a small standard deviation of ≈ 100 m/s that remains approximately the same for all loadings. This lack of spread in their speeds is most likely due to the reduced number of dislocation-to-dislocation interactions imposed by the natural cut-off distance of $c_l \times \Delta t$ (i.e., the distance the longitudinal wavefront of a dislocation must travel to reach another within the time interval Δt): within the timescale of the simulation, most dislocations interact only with their nearest neighbours. As the simulations advance and the dislocation-to-dislocation interactions begin to affect both sources and existing dislocations, the average speed tends to slowly decrease (from $M_t \approx 0.34$ at $t=50$ ps down to $M_t \approx 0.28$ for 1 GPa at 100 ps); this is consistent with the increased plastic hardening expected in these circumstances (Gurrutxaga-Lerma et al., 2015d). Since at those the elastodynamic fields of dislocations do not display strong Doppler-like contractions, their magnitude once the transverse wave front has arrived at a given point will be very similar to that of the elastostatic counterparts at those speeds (Gurrutxaga-Lerma et al., 2013); this explains why the plastic response in the background region is similar to both the elastodynamic and elastostatic cases.

In region III, i.e., the area surrounding the crack tip, the picture is rather different. For one thing, the average speed of dislocations in that region is $M_t \approx 0.85$–0.95 irrespective of the loading, although dislocation speeds tend to decrease quickly as they move away from the crack tip, down to the speeds reported for above for the background region. As a result, the fields of the fast moving, crack tip dislocations display the Doppler-like contractions and magnifications characteristic of the

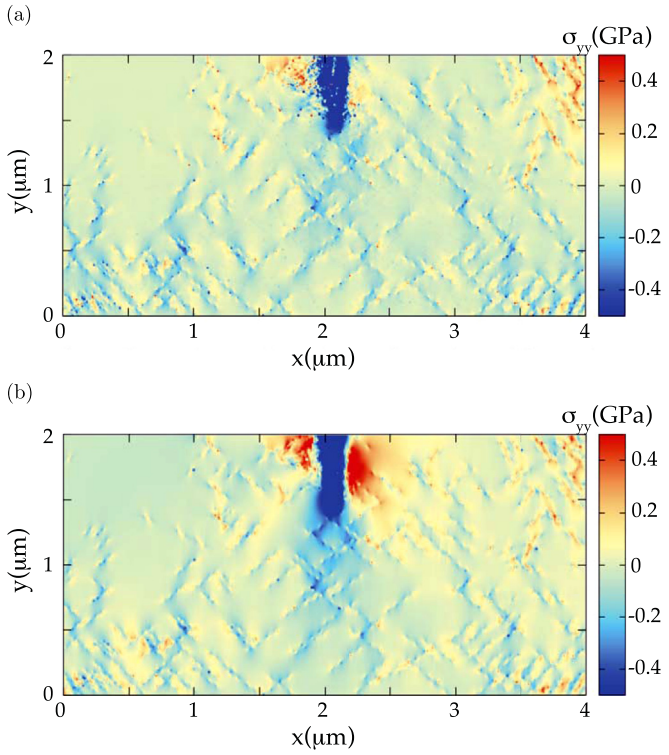

Fig. 4. σ_{yy} fields due to dislocations in the elastodynamic and elastostatic cases. (a) σ_{yy} fields due to dislocations at $t=100$ ps and $P=1$ GPa, as obtained from D3P. (b) Corresponding elastostatic σ_{yy} fields due to dislocations at $t=100$ ps and $P=1$ GPa.

elastodynamic dislocation (Gurrutxaga-Lerma et al., 2014), causing more localised shielding.

The effect of anti-shielding dislocations in these simulations is minimal, not only because of there are fewer of them compared to the elastostatic case, but also because their residence time before reaching a free surface is short. The applied stress that drives dislocations towards free surfaces is higher than in elastostatic, lower stress applications, and there are additional inertial effects that, as shown in Gurrutxaga-Lerma et al. (2015c), in fact magnify the image forces which accelerates dislocations towards the free surfaces. In contrast, the shielding dislocations see their residence time around the crack tip increased, because as they move further away from the tip the magnitude of the driving force decreases, and the magnitude of the contracted elastodynamic image force is larger (Gurrutxaga-Lerma et al., 2015c).

The elastodynamic mode I crack tip field is known to evolve as (Freund, 1989)

$$\sigma_{yy} = \frac{K_I(t)}{\sqrt{2\pi x}} \tag{7}$$

where x is the distance to the crack tip, and $K_I(t) \propto P\sqrt{t}$ (Freund, 1989) is the time-dependent stress intensity factor for a stationary mode I crack. Thus, by fitting the computed relaxation of σ_{yy} to a $1/\sqrt{x}$, the magnitude of the crack tip shielding can be estimated (see Fig. 4).

Fig. 5 shows the time evolution of the plastic shielding of $K_I(t)$ over time averaged over 5 simulations in each case to de-emphasise the effect of local fluctuations, with the variation indicated by error bars. This serves as a measure of the effectiveness of elastodynamic dislocations in shielding the crack tip. Necessarily, this shielding is negative, i.e., compressive, showing that the dislocations tend to plastically relax the tensile field induced by the loaded crack tip. The main characteristic of the observed plastic shielding is that it increases in time (i.e., it becomes more compressive). This effect is not dissimilar to the attenuation of the dynamic yield point described in Gurrutxaga-Lerma et al. (2015a), whereby the elastodynamic fields of dislocations interfere, destructively in this case, with the elastodynamic fields of the crack tip, causing an attenuation of the yield point of the material; in this case, the observed time evolution of the attenuation of $K_I(t)$ would entail that the apparent fracture toughness of the material increases over time. The causes of this are found in the continuous generation of new dislocations from the crack tip; as a shielding dislocation is emitted from the crack, it moves away from it, and its shielding effect decays until a new dislocation is emitted. Since the fields of an elastodynamic dislocation are weaker behind the core (relative to the direction of motion) (Gurrutxaga-Lerma et al., 2013, 2014), this process of emission does not saturate as readily as it would for static dislocations, and contributes to the observed accumulation of shielding over time.

As it does in the elastic case, the shielding of $K_I(t)$ increases in proportion to $\sqrt{t}$ (vid. Freund, 1989); this is deduced by

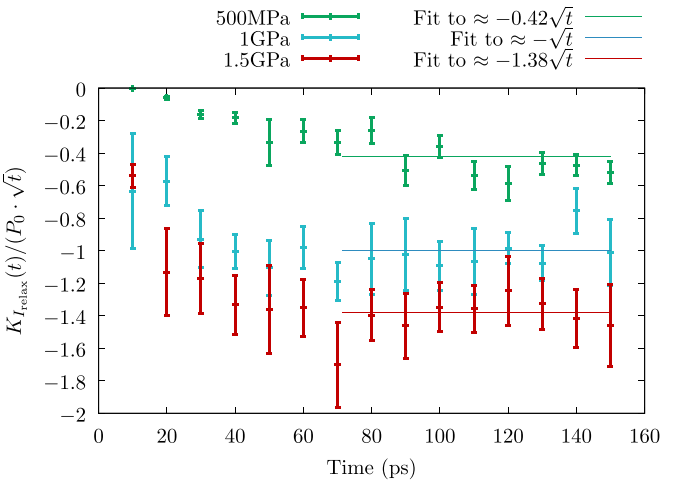

Fig. 5. Attenuation of K_I by the dislocations, for different loadings. The relaxed $K_{I_{\text{relax}}}$ is normalised with respect to $P_0\sqrt{t}$, where here $P_0 = 1$ GPa is chosen to enable a better comparison between different load magnitudes. In general, the magnitude of the attenuation of $K_I(t)$ increases in proportion to $\sqrt{t}$, as shown by the fits provided in the plot. Notice that the fits have also been normalised, so they are represented by straight lines.

fitting the evolution of the shielding of $K_I(t)$ to a $A \times \sqrt{t}$ function, where A is a fitting parameter and t the time. The attenuation of K_I in proportion to $\sqrt{t}$ shows that dislocations are generated in sufficient numbers to keep up with the elastic field of the crack tip (qv. Freund, 1989). Further to this, as can be seen in Fig. 5, the plastic shielding of the crack tip is approximately proportional to the magnitude of the external load; this is again consistent with the elastodynamic field of the stationary crack tip (Freund, 1989).

Our results show that the magnification of the elastodynamic fields of the crack tip (sometimes estimated to be around 25% higher than the static equivalent Kalthoff and Shockey, 1977; Homma et al., 1983) is accompanied by enhanced plastic shielding, which is consistent with the experimental observation that materials which are relatively strain rate insensitive in their bulk response but tend to fail in a locally ductile manner experience an increase in fracture toughness with crack speed (Freund, 1989). This generally applies to most FCC metals, including aluminium, which is the subject of this study (see for instance Shukla et al., 1988; Owen et al., 1998). In metals, this effect has been attributed to the interplay between inertial effects at the crack tip and the strain rate sensitivity of the material (Freund, 1989), in a way which appears to be consistent with the predictions of these simulations. In particular, Owen et al. (1998) showed that over short timescales the dynamic fracture toughness in thin films of FCC aluminium alloys was invariably larger than the equivalent static fracture toughness; they attributed this to inertial effects and small scale rate sensitive yielding taking place at the crack tip, which is entirely consistent with our results: we observe an elastodynamic enhancement of the plastic shielding relative to the elastostatic case (see Fig. 3), which leads to an increase in the dynamic fracture toughness of the material due to inertial effects affecting the yielding of the material around the crack tip.

4. Conclusions

This article has examined the shielding of a stationary mode I crack by elastodynamic dislocations over reduced time scales and under conditions representative of dynamic loading. Two dislocation generation mechanisms have been included: Frank–Read sources and homogeneous nucleation of dislocations at the crack tip. Using D3P, the dislocations have been treated as elastodynamic sources of elastic waves that in their generation and motion relax the crack tip. The effect that the elastodynamic dislocations have over the crack tip has been compared to the corresponding elastostatic case.

This study has shown that the elastodynamic shielding of the crack tip is produced primarily by fast moving dislocations nucleated at the crack tip. This is because of the retardation effects associated with dislocation-to-dislocation and dislocation-to-crack interactions in the elastodynamic case: for reduced timescales, only those dislocations in the immediate vicinity of the crack tip were able to contribute to the relaxation of the crack tip.

Most of these dislocations can only be generated homogeneously at the crack tip. Background dislocations generated by and moving away from Frank–Read sources have been shown to be produced in insufficient numbers to shield the crack tip. Crucially, the Frank–Read sources generated dislocations at a rate too slow to produce the necessary plastic shielding.

The resulting elastodynamic plastic shielding of the crack tip is shown to be considerably larger in magnitude than that in the corresponding elastostatic case, and increases over time. This is due to the dynamic magnification of the fields of fast moving dislocations. This affects both the crack tip and the crack path: in the elastostatic case, the corresponding dislocation configuration induced a tensile stress state ahead of the crack tip, which may be associated with microvoid formation and ductile fracture; this stress was absent in the elastodynamic description. This suggests that, over short timescales,

elastodynamic dislocations increase the material's apparent fracture toughness more than elastostatic dislocations, which is consistent with experimental observation (Owen et al., 1998).

Future work Gurrutxaga-Lerma et al. (2016) will focus on studying the effect dynamic shielding has on propagating cracks.

Acknowledgements and contributions

B.G.-L. conceived the mathematical models and wrote the paper. D.S.B., D.D. and A.P.S. interpreted the results and contributed to the writing of the discussions. All authors gave final approval for publication.

B.G.-L. acknowledges the support of the EPSRC via the EPSRC Doctoral Prize Fellowship program. The authors declare no competing interests. This work does not have any experimental data.

All simulation results are made available upon request by email to the corresponding author.

References

Aubry, S., Kang, K., Ryu, S., Cai, W., 2011. Energy barrier for homogeneous dislocation nucleation: comparing atomistic and continuum models. Scr. Mater. 64, 1043–1046.
Balint, D.S., Deshpande, V.S., Needleman, A., Van der Giessen, E., 2005. Discrete dislocation plasticity analysis of crack-tip fields in polycrystalline materials. Philos. Mag. 85 (2627), 3047–3071.
Balint, D.S., Deshpande, V.S., Needleman, A., Van der Giessen, E., 2006. Size effects in uniaxial deformation of single and polycrystals: a discrete plasticity analysis. Model. Simul. Mater. Sci. Eng. 14, 409–442.
Benzerga, A.A., 2008. An analysis of exhaustion hardening in micron-scale plasticity. Int. J. Plast. 24, 1128–1157.
Benzerga, A., 2009. Micro-pillar plasticity: 2.5D mesoscopic simulations. J. Mech. Phys. Solids 57 (9), 1459–1469.
Benzerga, A.A., Bréchet, Y., Needleman, A., Van der Giessen, E., 2004. Incorporating three-dimensional mechanisms into two-dimensional dislocation dynamics. Model. Simul. Mater. Sci. Eng. 12, 159–196.
Brown, L.M., 1964. The self-stress of dislocations and the shape of extended nodes. Philos. Mag. 10 (105), 441–466.
Bulatov, V.V., Abraham, F.F., Kubin, L.P., Devincre, B., Yip, S., 1998. Connectic atomistic and mesoscale simulations of crystal plasticity. Nature 391, 669–672.
Cleveringa, H.H.M., Van der Giessen, E., Needleman, A., 2000. A discrete dislocation analysis of mode i crackgrowth. J. Mech. Phys. Solids 48, 1133–1157.
Davoudi, K.M., Nicola, L., Vlassak, J.J., 2014. Bauschinger effect in thin metal films: discrete dislocation dynamics study. J. Appl. Phys. 115 (1), 013507.
Freund, L.B., 1989. Dynamic Fracture Mechanics. Cambridge University Press, Cambridge, UK.
Freund, L.B., Hutchinson, J.W., 1985. High strain-rate crack growth in rate-dependent plastic solids. J. Mech. Phys. Solids 33 (2), 169–191.
George, A., Michot, G., 1993. Dislocation loops at crack tips: nucleation and growth—an experimental study in silicon. Mater. Sci. Eng. A 164, 118–134.
Gurrutxaga-Lerma, B., Balint, D.S., Dini, D., Eakins, D.E., Sutton, A.P., 2013. A dynamic discrete dislocation plasticity method for the simulation of plastic relaxation under shock loading. Proc. R. Soc. A 469, 20130141.
Gurrutxaga-Lerma, B., Balint, D.S., Dini, D., Eakins, D.E., Sutton, A.P., 2014. Dynamic Discrete Dislocation Plasticity. Advances in Applied Mechanics, vol. 47. Elsevier (Chapter 2).
Gurrutxaga-Lerma, B., Balint, D.S., Dini, D., Eakins, D.E., Sutton, A.P., 2015a. Attenuation of the dynamic yield point of shocked aluminum using elasto-dynamic simulations of dislocation dynamics. Phys. Rev. Lett. 114, 174301.
Gurrutxaga-Lerma, B., Balint, D.S., Dini, D., Eakins, D.E., Sutton, A.P., 2015b. The role of homogeneous nucleation in planar dynamic discrete dislocation plasticity. J. Appl. Mech. 82, 071008.
Gurrutxaga-Lerma, B., Balint, D.S., Dini, D., Sutton, A.P., 2015c. Elastodynamic image forces on dislocations. Proc. R. Soc. A 471 (2181), 20150433.
Gurrutxaga-Lerma, B., Balint, D.S., Dini, D., Sutton, A.P., 2015d. The mechanisms governing the activation of dislocation sources in aluminum at different strain rates. J. Mech. Phys. Solids. 84, 273–292, http://dx.doi.org/10.1016/j.jmps.2015.08.008.
Gurrutxaga-Lerma, B., Balint, D.S., Dini, D., Sutton, A.P., 2016. A dynamic discrete dislocation plasticity study of elastodynamic shielding of propagating cracks, in preparation.
Gutkin, M.Y., Ovidko, I.A., 2008. Homogeneous nucleation of dislocation loops in nanocrystalline metals and ceramics. Acta Mater. 56, 1642–1649.
Hirsch, P.B., Roberts, S.G., 1996. Comment on the brittle-to-ductile transition: a cooperative dislocation generation instability; dislocation dynamics and the strain-rate dependence of the transition temperature. Acta Mater. 44 (6), 2361–2371.
Hirsch, P.B., Roberts, S.G., Samuels, J., 1989. The brittle–ductile transition in silicon. II. Interpretation. Proc. R. Soc. A 421 (1860), 25–53.
Hirth, J.P., Lothe, J., 1982. Theory of Dislocations, 2nd edition. John Wiley & Sons, Malabar, FL, New York.
Holland, D., Marder, M., 1998. Ideal brittle fracture of silicon studied with molecular dynamics. Phys. Rev. Lett. 80 (4), 746.
Homma, H., Shockey, D.A., Murayama, Y., 1983. Response of cracks in structural materials to short pulse loads. J. Mech. Phys. Solids 31 (3), 261–279.
Jokl, M.L., Vitek, V., McMahon, C.J., 1980. A microscopic theory of brittle fracture in deformable solids: a relation between ideal work to fracture and plastic work. Acta Metall. 28, 1479–1488.
Jokl, M.L., Vitek, V., McMahon, C.J., Burgers, P., 1989. On the micromechanics of brittle fracture: existing vs injected cracks. Acta Metall. 37 (1), 87–97.
Kalthoff, J.F., Shockey, D.A., 1977. Instability of cracks under impulse loads. J. Appl. Phys. 48 (3), 986–993.
Kermode, J.R., Albaret, T., Sherman, D., Bernstein, N., Gumbsch, P., Payne, M.C., Csányi, G., De Vita, A., 2008. Low-speed fracture instabilities in a brittle crystal. Nature 455 (7217), 1224–1227.
Kermode, J.R., Ben-Bashat, L., Atrash, F., Cilliers, J.J., Sherman, D., De Vita, A., 2013. Macroscopic scattering of cracks initiated at single impurity atoms. Nat. Commun. 4.
Klepaczko, J.R., 1990. Dynamic crack initiation, some experimental methods and modelling. In: Klepaczko, J.R. (Ed.), Crack Dynamics in Metallic Materials. Springer, Vienna, pp. 255–453.
Loyola de Oliveira, M.A., Michot, G., 1998. Three dimensional analysis of the interaction between a crack and a dislocation loop. Acta Mater. 46 (4), 1371–1383.
Meyers, M.A., 1994. Dynamic Behavior of Materials. John Wiley, Hoboken, NJ.
Minor, A.M., Asif, S.A.S., Shan, Z., Stach, E.A., Cyrankowski, E., Wyrobek, T.J., Warren, O.L., 2006. A new view of the onset of plasticity during the nanoindentation of aluminium. Nat. Mater. 5 (9), 697–702.
Nicola, L., Van der Giessen, E., Needleman, A., 2001. 2D dislocation dynamics in thin metal layers. Mater. Sci. Eng. A 309, 274–277.
Nicola, L., Van der Giessen, E., Needleman, A., 2003. Discrete dislocation analysis of size effects in thin films. J. Appl. Phys. 93, 5920.
O'Day, M.P., Curtin, W.A., 2005. Bimaterial interface fracture: a discrete dislocation model. J. Mech. Phys. Solids 53 (359–382).
Olmsted, D.L., Hector, L.G., Curtin, W.A., Clifton, R.J., 2005. Atomistic simulations of dislocation mobility in Al, Ni and Al/Mg alloys. Model. Simul. Mater. Sci. Eng. 13, 371–388.

Owen, D.M., Zhuang, S., Rosakis, A.J., Ravichandran, G., 1998. Experimental determination of dynamic crack initiation and propagation fracture toughness in thin aluminum sheets. Int. J. Fract. 90 (1–2), 153–174.
Rice, J.R., 1987. Tensile crack tip fields in elastic–ideally plastic crystals. Mech. Mater. 6, 317–335.
Rice, J.R., Beltz, G.E., 1994. The activation energy for a dislocation nucleation at a crack. J. Mech. Phys. Solids 42 (2), 333–360.
Rice, J.R., Thomson, R., 1974. Ductile versus brittle behaviour of crystals. Philos. Mag. 29 (1), 73–97.
Samuels, J., Roberts, S.G., 1989. The brittle–ductile transition in silicon. I. Experiments. Proc. R. Soc. A 421 (1860), 1–23.
Shishvan, S.S., Van der Giessen, E., 2010. Distribution of dislocation source length and the size dependent yield strength in freestanding thin films. J. Mech. Phys. Solids 58 (5), 678–685.
Shukla, A., Agarwal, R.K., Nigam, H., 1988. Dynamic fracture studies on 7075-T6 aluminum and 4340 steel using strain gages and photoelastic coatings. Eng. Fract. Mech. 31 (3), 501–515.
Thompson, A.W., 1987. Modeling of local strains in ductile fracture. Metall. Trans. A 18 (11), 1877–1886.
Thomson, R., 1986. Physics of Fracture. Solid State Physics. vol. 39. Academic Press, London1–129.
Tschopp, M.A., McDowell, D.L., 2007. Tension–compression asymmetry in homogeneous dislocation nucleation in single crystal copper. Appl. Phys. Lett. 90 (12), 121916.
Tschopp, M.A., McDowell, D.L., 2008. Influence of single crystal orientation on homogeneous dislocation nucleation under uniaxial loading. J. Mech. Phys. Solids 56, 1806–1830.
Tvergaard, V., Hutchinson, J.W., 1992. The relation between crack growth resistance and fracture process parameters in elastic-plastic solids. J. Mech. Phys. Solids 40 (6), 1377–1397.
Van der Giessen, E., Needleman, A., 1995. Discrete dislocation plasticity: a simple planar model. Model. Simul. Mater. Sci. Eng. 3 (5), 689–735.
Xu, G., Argon, A.S., 2000. Homogeneous nucleation of dislocation loops under stress in perfect crystals. Philos. Mag. Lett. 80 (9), 605–611.
Xu, G., Argon, A.S., Ortiz, M., 1997. Critical configurations for dislocation nucleation from crack tips. Philos. Mag. A 75 (2), 341–367.
Zhu, T., Li, J., Yip, S., 2004. Atomistic study of dislocation loop emission from a crack tip. Phys. Rev. Lett. 93 (2), 025503.